Composites Science and Technology 191 (2020) 108079

Contents lists available at ScienceDirect

Composites Science and Technology

journal homepage: http://www.elsevier.com/locate/compscitech

# The magneto-mechanical properties of off-axis anisotropic magnetorheological elastomers

Jingyi Zhang, Haoming Pang, Yu Wang **, Xinglong Gong *

*CAS Key Laboratory of Mechanical Behavior and Design of Materials, Department of Modern Mechanics, CAS Center for Excellence in Complex System Mechanics, University of Science and Technology of China, Hefei, Anhui, 230027, China*

ARTICLE INFO

*Keywords:*
Anisotropic
Magnetorheological
Mechanical properties
Magnetic properties

ABSTRACT

Off-axis anisotropic magnetorheological (MR) elastomers with different particle chain orientations were investigated. Under the quasi-static and oscillatory shear excitation, the internal structure has significant effects on the mechanical response (initial modulus, magneto-induced modulus and magneto-deformation). The MR effect of the anisotropic MR elastomers could be increased by 127% through simply changing the particle chain orientation by 15° during the fabrication process. The experimental results were verified by using a modified magnetic dipole theoretical model. The magneto-induced torque and normal force of the anisotropic MR elastomers could be significantly affected by the orientation of particle chain, which had great guiding significance for practical applications. Moreover, the MR elastomer composites could achieve complex three-dimensional origami deformations under the external magnetic field. The capability to control the shape morphing of this off-axis anisotropic MR elastomer might open new opportunities for programming complex soft structures.

## 1. Introduction

Magnetorheological (MR) elastomers are composite materials with magnetic particles embedded into a compliant elastomer matrix. In general, MR elastomers can be categorized into two types regarding the distribution of magnetic particles with the elastomer matrix. Based on whether the magnetic particles are either in chain by aligning to a specific direction or randomly distributed inside the polymeric matrices, they are termed as anisotropic and isotropic MR elastomers, respectively [1]. Owing to their controllable and reversible mechanical performance under external magnetic field, MR elastomers have found widespread industrial applications, such as aerospace [2], automotive [3,4], civil and electrical engineering [5,6], motion and vibration control [7–9].

Besides the field-dependent modulus and damping [10,11], the deformation property of MR elastomers is also an important issue ensuring their applications [12,13]. Compared with the traditional giant magnetostrictive materials such as Terfenol-D (T-D) which is a magnetostrictive alloy of terbium, dysprosium and iron, the benefits of using MR elastomers are not only in reducing the rising costs associated with dwindling supplies of rare earth metals, but also in increasing the ability to mould to the desired structural shapes [14,15] for the applications in soft robot [7,16], soft actuator [17–19] and artificial muscle [20], etc. Tsumori et al. [21] fabricated the magnetically actuated artificial cilia for use as a pump in the microelectro-mechanical systems by additive manufacturing methods. They developed a magnetic actuator by anisotropic MR elastomers contained with soft magnetic particle chain structures. The movement of the artificial cilium could be controlled by the orientation of the multiparticle chains. Guan et al. [12] studied on the elongation of MR elastomers with CIPs dispersed in silicon rubber. They found that the orientation of the particle chain significantly influenced the magnetostrictive performance of MR elastomers and the microstructure was the primary driver of the deformation behaviors of MR elastomers.

More particularly, the MR elastomers can exhibit length and volume changes in homogeneous magnetic field. This effect is traditionally associated with magnetostriction, which is depended on the orientation of magnetic particles and their spatial relationship in the polymer matrix [22]. It has been proved that MR elastomers can be tailored for exhibiting very high coupling between the magnetic and the mechanical behaviors by the inclusion of oriented particles within the elastomers matrix [23–27]. Tian et al. [28] fabricated the MR elastomers with 45° carbonyl iron particles (CIPs) aligned to the applied magnetic field. They

* Corresponding author.
** Corresponding author.
*E-mail addresses:* wyu@ustc.edu.cn (Y. Wang), gongxl@ustc.edu.cn (X. Gong).

https://doi.org/10.1016/j.compscitech.2020.108079
Received 17 September 2019; Received in revised form 4 January 2020; Accepted 16 February 2020
Available online 21 February 2020

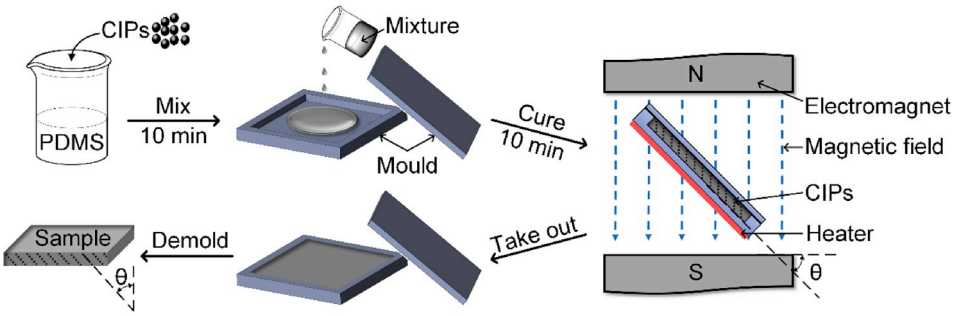


**Fig. 1.** Illustration of the fabrication process for MR elastomer sample.

found that the storage modulus along the compression direction of the particle chain was higher than that along the tensile direction of the particle chain. Boczkowska et al. [29] examined the MR elastomers consisting of CIPs in a polyurethane matrix and noted that the highest increase in storage modulus was obtained for samples with 30° particle distribution. However, only little research work concerns on the relationship between the arrangement of magnetic particle chain and the magneto-mechanical properties.

In this study, several novel anisotropic MR elastomers were fabricated by embedding preliminary off-axis aligned magnetizable particles, which was obtained by applying an external magnetic field during the elaboration process of the materials. The relationships between the orientation of magnetic particle chains and the mechanical properties of MR elastomers were explored. A modified magnetic dipole theoretical model was proposed to explain the anisotropic magneto-mechanical behaviors. Finally, some special double-layer composite structures combined with special anisotropic MR elastomers film and PDMS film were used to demonstrate the magneto-deformation behaviors under the external magnetic field.

## 2. Experiments

### 2.1. Materials

The materials used to manufacture the MR elastomers were polydimethylsiloxane (PDMS) precursor and curing agent (Sylgard 184), all purchased from Dow Corning. Based on previous studies [28,30,31], the MR elastomers fabricated from PDMS had relatively small stiffness, which was benefit for magneto-induced behaviors. The spherical CIPs, with an average size of 7 μm, were purchased from BASF in Germany. All the reagents were analytically pure and were used without additional purification.

### 2.2. Preparation

Firstly, a total of 16 g of CIPs and 1 g of PDMS curing agent were added into 15 g of PDMS precursor. The mixture was stirred for 10 min with a glass rod to make the CIPs well dispersed. Then, the mixture was transferred to a mould sized 50 mm × 50 mm × 1 mm, and degassed in a vacuum container for 10 min to remove the trapped bubbles. After that, the mixture was cured at 100 °C for 10 min under an external magnetic field of 1 T. During the vulcanization process, the CIPs were rearranged along the direction of the external magnetic field under the influence of magnetic interactions between the particles. By varying the spatial orientation of the mould in the magnetic field, samples with different internal particle chain orientations could be fabricated (Fig. 1). If the angle of the normal direction of the mould to the direction of the external magnetic field is θ, the MR elastomer sample is defined as A-MRE-θ. In this work, several samples with θ of 0°, 5°, 10°, and 15° were prepared. According to the experiment requirement, the sample was cut into sizes of 7 mm × 7 mm × 1 mm and 3 mm × 3 mm × 1 mm.

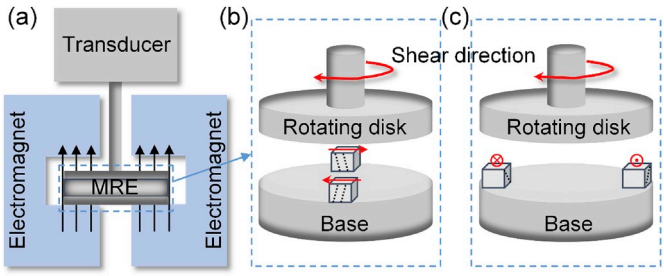


**Fig. 2.** (a) Schematic illustration of the rheometer with magnetic coil device; relative position of the sample to the base of the rheometer: (b) front view, (c) left view.

### 2.3. Characterization and testing system

The microstructures of the samples were observed by an environmental scanning electron microscope (Gemini SEM 500, Zeiss). The accelerating voltage was 20 kV.

The mechanical behaviors of the different samples were measured by using a rheometer (Physica MCR 301, Anton Paar Co., Austria). As shown in Fig. 2a, the external adjustable magnetic field was applied along the normal direction of the sample. Magnetic flux density could vary from 0 T to 0.8 T. For A-MRE-θ (θ > 0°), the angle between the internal particle chain and the shear direction of the sample at different positions was different during the rotary shearing process. The sample was thus sliced and placed symmetrically to ensure that the angle between the particle chain and the shear direction was basically the same as shown in Fig. 2b and c. The relationship between rheometer data was discussed in support information (S1).

## 3. Results and discussion

After the fabrication, the microstructures for different MR elastomer samples were employed by SEM, which is shown in Fig. 3. The magnification of Fig. 3a–d and Fig. 3e–h is 150 and 1000 times, respectively. The white spots are the CIPs. And Fig. 3e–h are the enlargement views of the squares in Fig. 3a–d, respectively. The x axis is parallel to the sample edge, and the y axis is along the thickness of the sample. Since all the samples are anisotropic, the CIPs form chain structure in the matrix. Because of the magnetism, the CIPs move in the matrix to form chains along the direction of the external magnetic field during the curing process. Therefore, it can be seen that the chain directions in Fig. 3e–h are basically the same as the pre-design orientations.

The steady shear was applied on the samples with different magnetic particle chain orientations. The shear strain was applied along the clockwise direction in the rheometer and defined as positive shear strain. The shear strain was 1% and the shear strain rate was 0.001 $s^{-1}$. A pre-pressure was exerted on the sample to avoid the sliding between the rotating disk and the sample. As can be seen from Fig. 4a, the initial

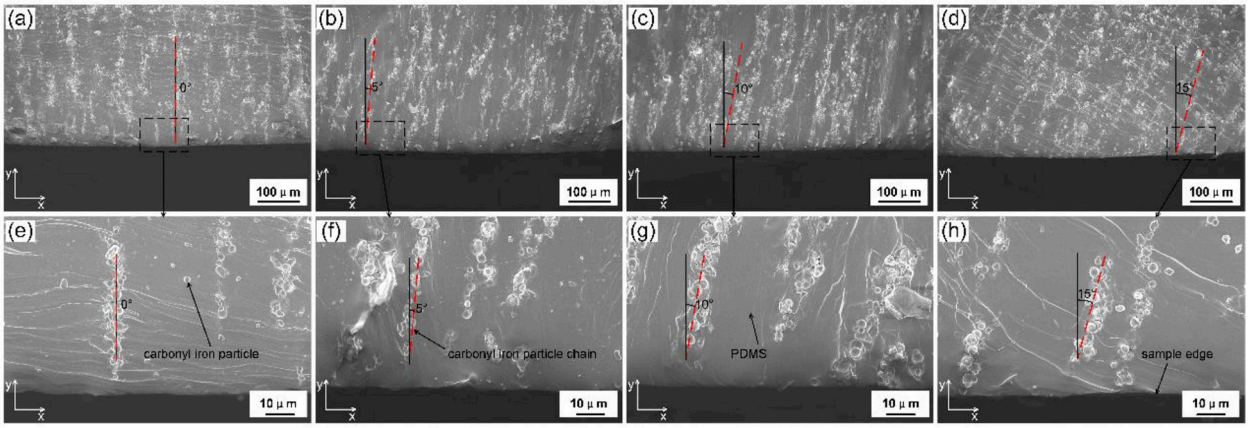


**Fig. 3.** SEM images of the samples: (a, e) A-MRE-0°; (b, f) A-MRE-5°; (c, g) A-MRE-10°; (d, h) A-MRE-15°.

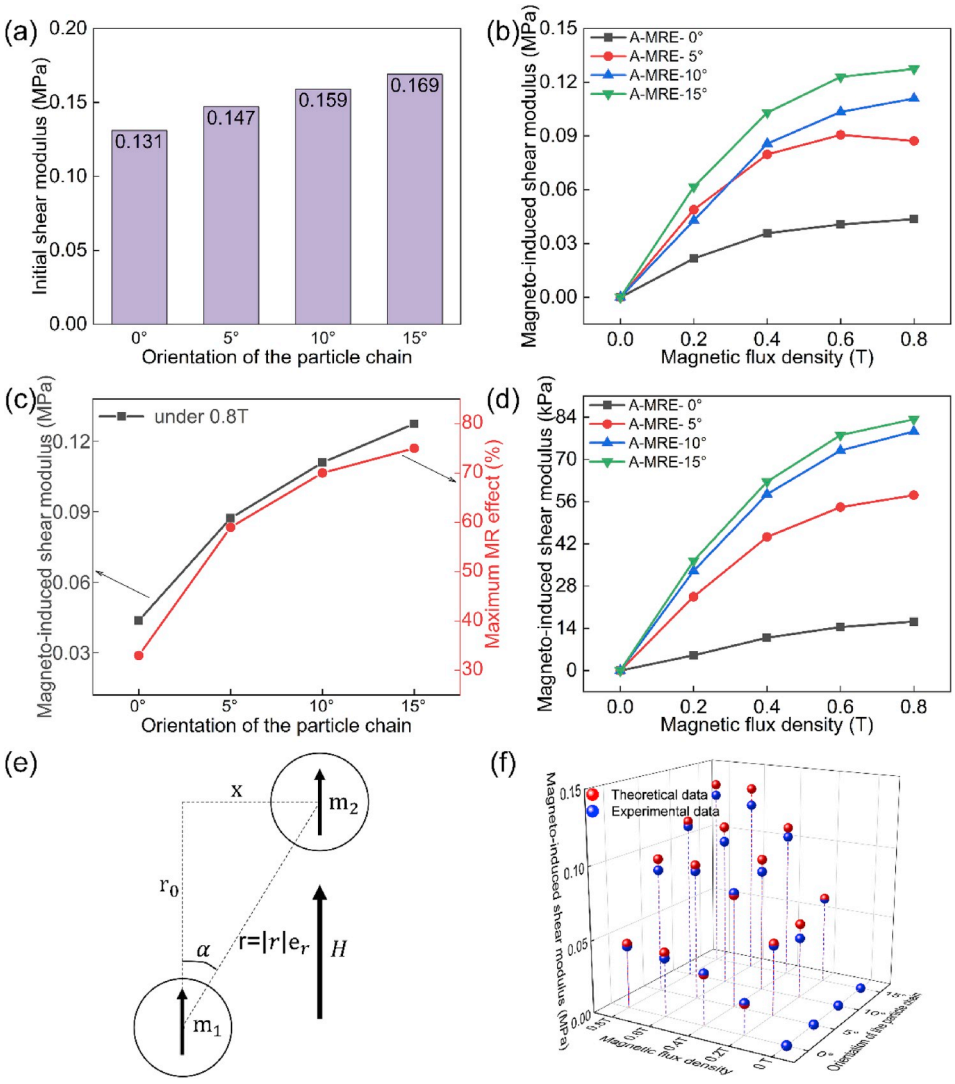


**Fig. 4.** Quasi-static one-way shear of four samples with different angles under shear strain 1%: (a) initial shear modulus, (b) magneto-induced shear modulus under different magnetic flux densities, (c) magneto-induced shear modulus at 0.8 T and maximum MR effect; (d) the relationship between magneto-induced shear modulus and magnetic flux density under shear strain 10%; (e) magnetic interaction of two particles modeled as dipole moments; (f) comparison of theoretical results with experimental results under shear strain 1%.

shear modulus of different samples is plotted. It could be concluded that the larger the angle, the greater the initial shear modulus. The magneto-induced shear modulus was defined as the difference between the shear modulus under the external magnetic field and that under zero magnetic field. Fig. 4b shows that the magneto-induced shear modulus of all samples increases with the magnetic flux density increasing. And it also presents that, under the same magnetic flux density, the magneto-induced shear modulus is greater for the larger orientation angle of the magnetic particle chain. The MR effect was defined as the ratio of the magneto-induced shear modulus to the shear modulus under zero magnetic field. The magneto-induced shear modulus and the MR effect for different samples under magnetic flux density of 0.8 T are

summarized in Fig. 4c. It could be obtained that the MR effect of the A-MRE-0° sample was 33%, while the MR effect of the A-MRE-15° sample could increase to 75%. If the shear strain increased to 10%, similar trend as in Fig. 4b was emerged with the magnetic flux densities varying and the magneto-induced shear modulus was reduced accordingly (Fig. 4d).

A modified quasi-static dipole model was proposed here to analysis the variation of magneto-induced shear modulus. According to Rosensweig's theory [32], two adjacent particles (dipoles) in a particle chain and the applied magnetic field H are illustrated in Fig. 4e. The interaction energy between the dipoles $m_1$and $m_2$can be expressed as:

$$E_{12} = \frac{1}{4\pi\mu_1\mu_0}\left[\frac{m_1 \cdot m_2 - 3(m_1 \cdot e_r)(m_2 \cdot e_r)}{|r|^3}\right] \tag{1}$$

where $\mu_0$ is the vacuum permeability, $\mu_1$ is the relative permeability of the matrix and $e_r$ is the unit vector of the point dipole center line formed by the two spherical particles, respectively. When the dipole moments are of identical direction and strength $|m|$, the equation (1) becomes:

$$E_{12} = \frac{|m|^2(1 - 3cos^2\alpha)}{4\pi\mu_1\mu_0|r|^3} = \frac{|m|^2\left(1 - 3\frac{r_0^2}{r_0^2+x^2}\right)}{4\pi\mu_1\mu_0(r_0^2 + x^2)^{3/2}} \tag{2}$$

in which $r_0$ and x are the distances of the two dipoles in parallel and perpendicular to the direction of the dipole moment, respectively. And here α is the angle between the $e_r$ unit vector and the direction of the dipole moment, which satisfies the following form:

$$tan\alpha = \tan(\theta + \gamma) = \frac{x}{r_0} \tag{3}$$

where θ is the initial angle between the $e_r$ unit vector and the external magnetic field, and γ is the shear strain of the particle chains. Then, the equation (2) comes into:

$$E_{12} = \frac{|m|^2(tan^2\alpha - 2)}{4\pi\mu_1\mu_0 r_0^3(tan^2\alpha + 1)^{5/2}} \tag{4}$$

Here, the volume of the MR elastomer is $V_c$ and the volume fraction of CIPs in elastomer is $\varphi$. The total number of CIPs is n. If the diameter of the single magnetic particle is d and the volume is $V_i$, the total number of CIPs can be expressed as:

$$n = \varphi\frac{V_c}{V_i} = \varphi\frac{6V_c}{\pi d^3} \tag{5}$$

If it's assumed that the magnetic interaction only occurs between adjacent particles within a chain, the total energy density can be given as follows:

$$U = \frac{n}{V_c}E_{12} = \frac{3\varphi|m|^2(tan^2\alpha - 2)}{2\pi^2\mu_1\mu_0 d^3 r_0^3(tan^2\alpha + 1)^{5/2}} \tag{6}$$

Thus, the shear stress by the application can be computed by taking the derivative of the inter-particle energy density with respect to strain:

$$\tau = \frac{\partial}{\partial\gamma}U = \frac{\partial\alpha}{\partial\gamma}\frac{\partial tan\alpha}{\partial\alpha}\frac{\partial}{\partial tan\alpha}U = \frac{9\varphi|m|^2(4 - tan^2\alpha)tan\alpha}{2\pi^2\mu_1\mu_0 d^3 r_0^3(tan^2\alpha + 1)^{\frac{7}{2}}cos^2\alpha} \tag{7}$$

The equation (7) shows that τ increases with α increasing when α is within certain range. Therefore, if the shear strain γ is the same, the larger the initial angle θ would induce larger τ and larger shear modulus.

Furtherly, the induced particle polarization is the dipole moment magnitude per unit particle volume, which means $|m| = J_p V_i$, where $J_p$ is the induced particle polarization. As a result, the equation (7) becomes:

$$\tau = \frac{J_p^2\varphi(4 - tan^2\alpha)tan\alpha}{8\mu_1\mu_0 h^3(tan^2\alpha + 1)^{\frac{7}{2}}cos^2\alpha} \tag{8}$$

**Table 1**
Theoretical calculation parameters.

| | |
|---|---|
| Saturation polarization of the CIPs $J_s$ | 2.1 T |
| Carbonyl iron powder volume fraction ϕ | 0.11 |
| Result correction parameter k | 7 |
| Particle spacing parameter on particle chain h | 1.1 |
| Vacuum permeability $\mu_0$ | $4\pi \times 10^{-7}$ $T{\cdot}m/A$ |
| Matrix permeability $\mu_1$ | 1 |

where $h = r_0/d$ is defined to describe the mean gap between particles in a chain.

To obtain the induced particle polarization $J_p$, here the particle saturation model is adopted. Here c is the saturated ratio of the particle and is expressed as according to Jolly's work [33]:

$$c = \frac{(3 - 2/\varphi) \pm \left((3 - 2/\varphi)^2 + 12k((2 - 2kB/B_s)/\varphi + 3(k - 1))\right)^{1/2}}{6k} \tag{9}$$

where k is the possibility of interaction between the particle chains. B is the magnetic flux density of the applied magnetic field and the magnetic flux density in saturated particles region could be expressed as:

$$B_s = J_S + \frac{B - \varphi(1 - c^3)J_S}{1 + (3\varphi(c - c^3))/2} \tag{10}$$

where $J_s$ is the particle saturation polarization. Thus c can be derived from equations (9) and (10), in which $0 \le c \le 1$. Then, the induced particle polarization $J_p$ could be calculated:

$$J_p = \frac{(3B(c - c^3))/2 + (1 - c^3)J_S}{1 + (3\varphi(c - c^3))/2} \tag{11}$$

Finally, the magneto-induced shear stresses under different magnetic flux densities and strains can be derived by putting the $J_p$ into equation (8).

The comparison of theoretical results with experimental results when the shear strain is 1% is shown in Fig. 4f. Parameters used in theoretical calculations are listed in Table 1. The modeling results showed that the magneto-induced shear modulus of all samples increased with magnetic flux density and there was a higher magneto-induced shear modulus for the sample with large orientation angle under the same magnetic flux density. The theoretical results and the experimental results were fitting well.

And a further steady shear deformation along the anticlockwise was performed. Here, the clockwise deformation was recorded as N direction shear while the anticlockwise one was as P direction shear. As illuminated in Fig. 5a, whether the A-MRE-0° sample was sheared along the P direction or N direction, the inclination angle of the particle chains would be increased with the shear strain increasing. During the shear deformation, the average gap between the particles would be increased and the particle chains would be stretched. While for the A-MRE-θ (θ > 0°) sample (Fig. 5b), the inclination angle of the particle chains would be increased during the P direction shear. Instead, the inclination angle of the particle chains would be reduced during the N direction shear. The average gap between the particles and the particle chains also showed the opposite trend.

It could be found that the shear modulus in the N direction was higher than that in the P direction for all A-MRE-θ (θ > 0°) samples. While for the A-MRE-0° sample, the shear modulus was almost same in both directions (Fig. 5c and d). According to the theory modeling, the shear stress would increase when the average gap between the particles reduced. Therefore, for all the A-MRE-θ (θ > 0°) sample, shear along the N direction would lead the shear modulus increasing rather than along the P direction.

In addition, the oscillating shear experiment was performed on all

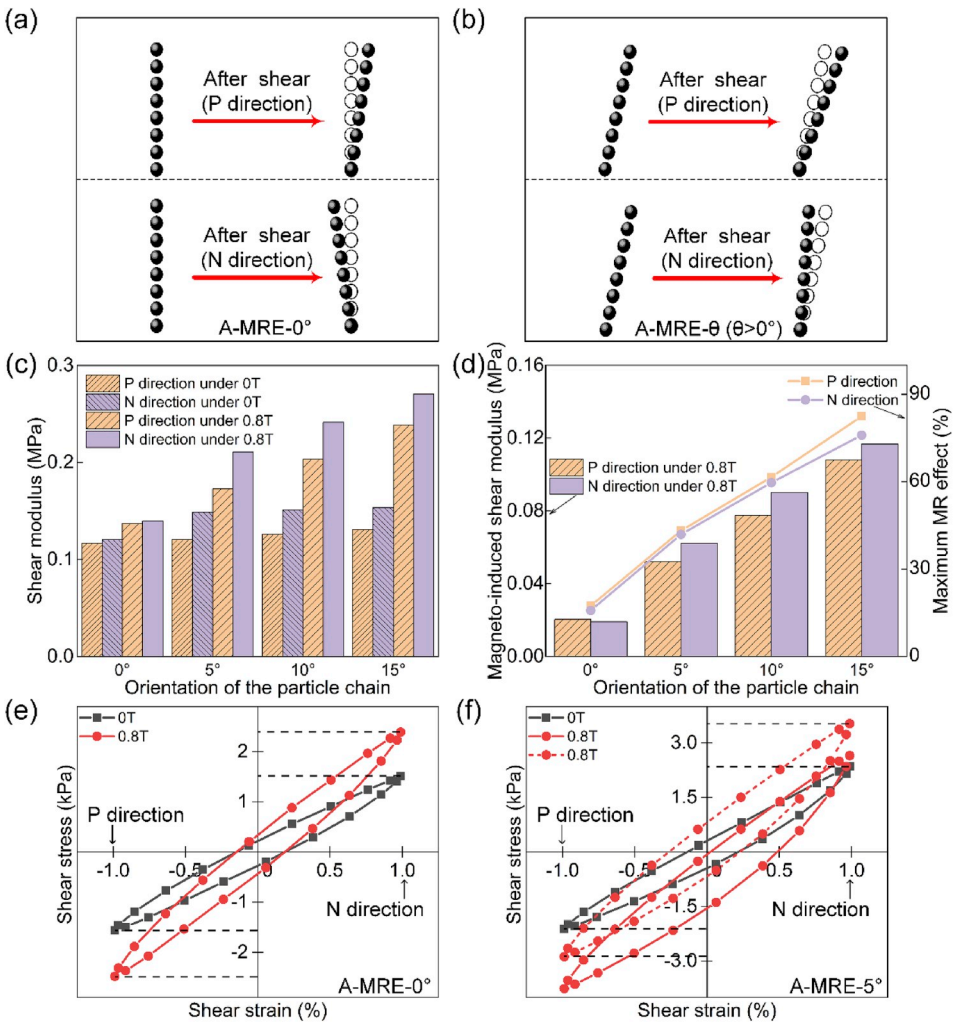


**Fig. 5.** The changes of the particle chain directions when sheared in P direction and N direction: (a) the A-MRE-0° sample, (b) the A-MRE-θ (θ > 0°) sample; P direction and N direction quasi-static shear of the samples (3 mm × 3 mm × 1 mm × 2): (c) shear modulus at 0 T and 0.8 T, (d) magneto-induced shear modulus at 0.8 T and maximum MR effect; the relationships between shear stress and shear strain of the samples (3 mm × 3 mm × 1 mm × 2) under oscillation shear: (e) the A-MRE-0° sample, (f) the A-MRE-5° sample.

samples under the same varied external magnetic field. Here, the results for A-MRE-0° and A-MRE-5° are plotted in the Fig. 5e and f for comparison. The storage modulus and loss modulus of the sample can be obtained from the slope and area of the stress–strain loop. They are the real and imaginary parts of the composite modulus. It indicated that the initial composite modulus of A-MRE-5° was greater than that of A-MRE-0°. For comparison, the curve of the A-MRE-5° sample under 0.8 T was shifted upwards as dotted line in Fig. 5f. It could be seen that the curves of the A-MRE-0° sample shearing in the N and P directions were symmetric about the origin under the applied magnetic fields of 0 T and 0.8 T. However, for the A-MRE-5° sample, the curve in the N direction was steeper than that in the P direction. The A-MRE-θ showed a typical asymmetrical mechanical properties. To investigate the durability of the orientation angle, the oscillation cycle shear tests were carried out with and without the external magnetic field (Fig. S2). The results showed that after 100 cycles, the relationship of shear stress and shear strain was unchanged.

Due to the special anisotropy magneto-induced mechanical behaviors, a steady magnetic field was applied on the sample in the rheometer without any shear deformation, as plotted in Fig. 6a. It could be found that, with the external magnetic field exerted, there would be a torque generated as for the sample A-MRE-5°, A-MRE-10° and A-MRE-15°. While for the sample A-MRE-0°, there was only a slight torque emerged. With the magnetic flux density increasing, the torque increased for all the samples. At the same time, it was also be detected that there was a variation of normal force for all the samples (Fig. 6b). The results showed that the variation was more inclined for the bigger orientation. The variation of the normal force with the external magnetic field changed was also studied (Fig. S3). It could be found that the coil response time was less than 0.1 ms, which could be ignored comparing with the response time of pure materials [34,35]. At the same time, the response time to 0.4 T magnetic field was around 73 ms, increasing with the precompression force. Moreover, Fig. S4 manifested that the change of normal force was stable after 1200 cycles of the on-off magnetic field. Fig. 6c shows an inclined chain-like structure in the MR elastomers. With the application of a magnetic excitation along the thickness, particle chains got magnetized and had a tendency to align themselves parallel to the magnetic field lines. Therefore, a counter-rotation would be created with the external magnetic field exerted and further made the whole sample create a counter-torque due to the interaction between particles and the polymer matrix. If the constraint was released, there would be a torsional deformation for the anisotropic MR elastomers under external magnetic field. In order to confirm that, a rectangular strip created by A-MRE-15° was put on the electromagnet platform. With the magnetic flux density increasing, it could be found that the strip inclined and reached the maximum inclined angle when the external magnetic flux density was about 45 mT. The relationship between the magnetic flux density and the inclined angle during the loading and unloading process is plotted in Fig. 6d. In loading process, the strip needed to overcome the adhesive force between the strip and the platform. Therefore, the strip started to incline until the external magnetic field was about 26 mT. Moreover, the strip under magnetic field could reach the maximum inclined angle 53.5°, which was the result of its own

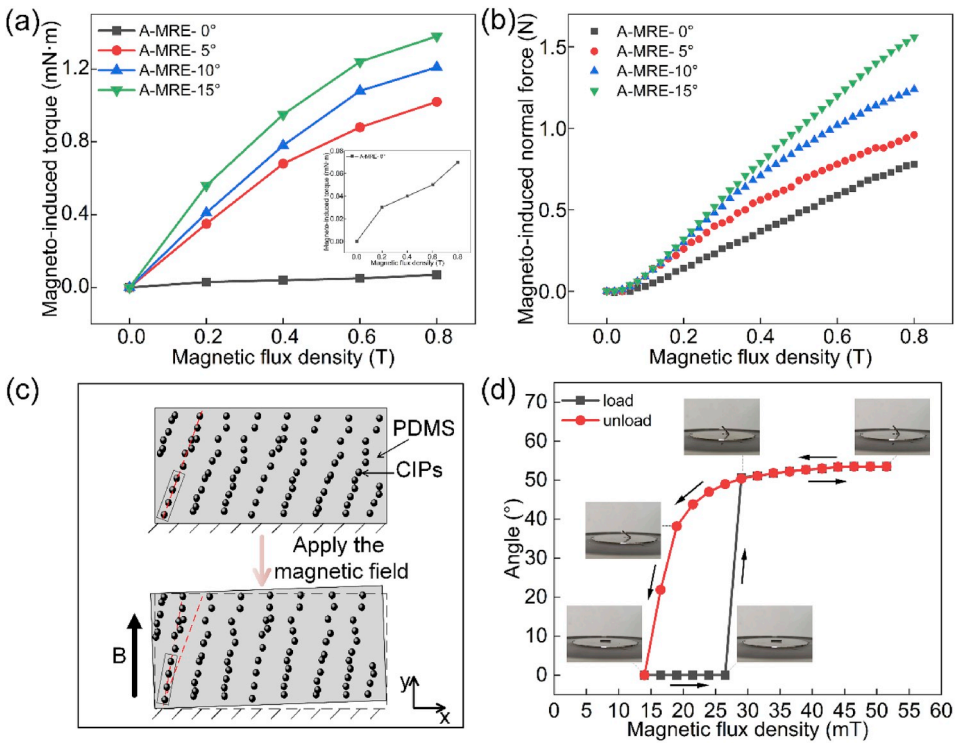


**Fig. 6.** The relationship of magneto-induced response and magnetic flux density under no shear: (a) magneto-induced torque, (b) magneto-induced normal force; (c) the deformation schematic of sample after applying the magnetic field; (d) the changes of off-plane displacement with the magnetic field.

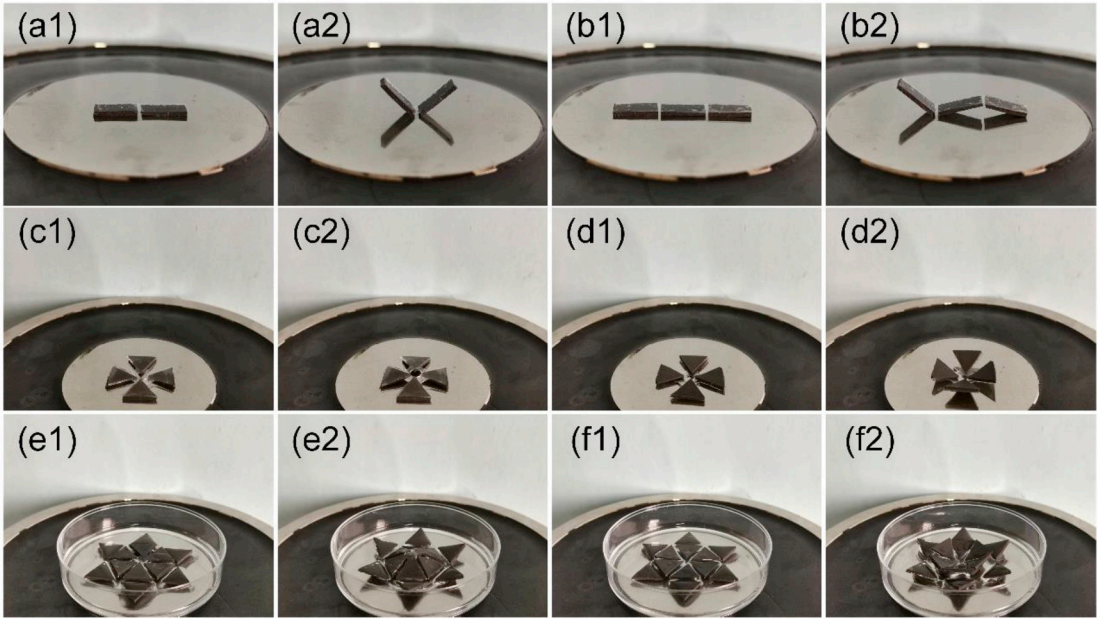


**Fig. 7.** Initial shape and deformation of different structures under a magnetic flux density of 77 mT: (a) two strips with symmetrical particle chain orientation, (b) three strips with alternate particle chain orientation, (c–d) four triangles distributed centrosymmetrically, (e–f) flower.

gravity and the emerging torque due to the magnetic field.

## 4. The magneto-deformation behaviors based on the off-axis anisotropic MR elastomer composite

As could be seen from above results, the MR elastomers with inclined particle chain had anisotropic mechanical properties and special out-plane deformation characteristic under the external magnetic field. Based on this discover, here a double-layer composite was designed to preliminary explore the magneto-deformation behaviors based on the off-axis anisotropic MR elastomers. Two methods were used to prepare the double-layer composite. The first one was to clean the sample surface with ethanol, and then stick the PDMS film on it by adhesion. The thickness of film was about 100 μm. The second method was to cut the sample into different shapes, and then put them into different shapes. After that, the PDMS solution was dripped onto the MR elastomer

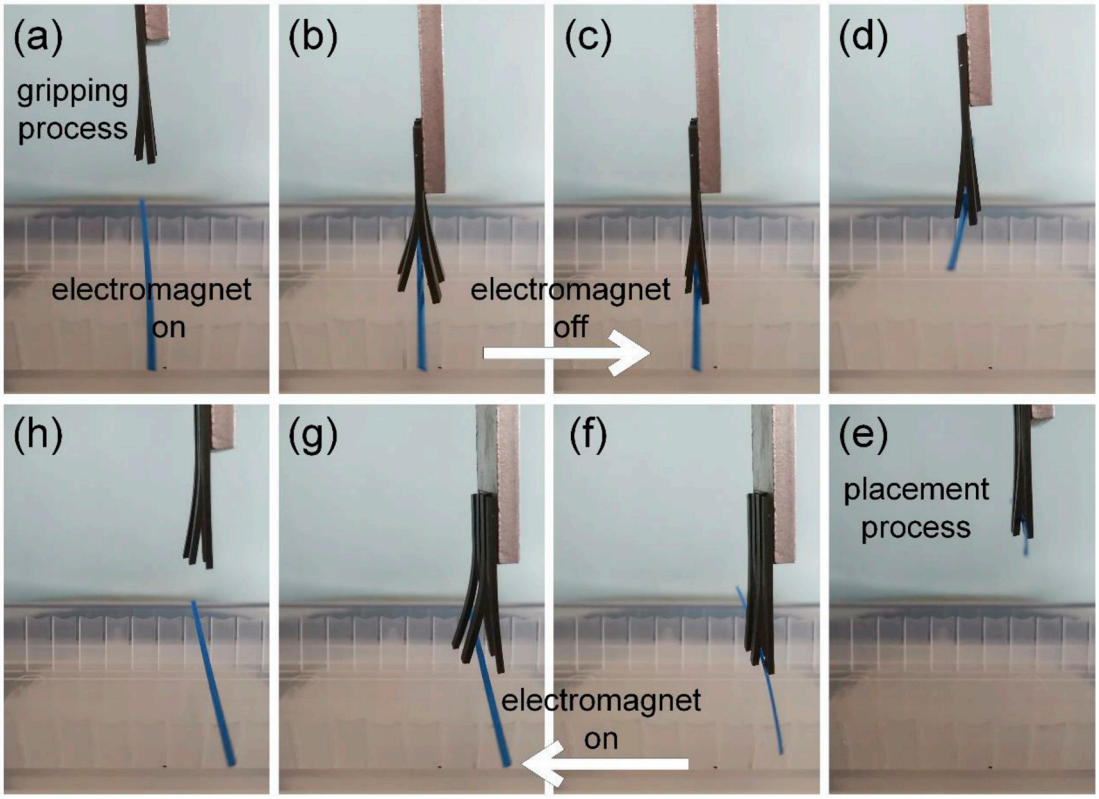


**Fig. 8.** Gripper: (a–d) the process of picking up an item, (e–h) the process of putting down the item.

surface. The final composite was gotten by vulcanized process.

After fabrication, various composite structures with A-MRE-15° sample combinations were designed. Fig. 7a1 manifests the structure spliced by two strips with symmetric distribution of particle chains. After applying magnetic flux density of 77 mT, the deformation is shown in Fig. 7a2. The structure that three strips arrange in a line becomes wavy after application of a magnetic field as shown in Fig. 7b. Fig. 7c and d show the structure that four triangles are distributed centrosymmetrically. It could be observed that when the PDMS was above, under the magnetic field, the structure was wrapped downward, but the structure was wrapped upward when the structure was turned over. Fig. 7e and f show the structure that is spliced in twelve triangles. Under the action of a magnetic field, the structure could be flower-like. And more structures are illustrated in Fig. S5.

A simple gripper was designed as shown in Fig. S6. The structure was consisted of four long strips, two of them were A-MRE-15° and the other two were A-MRE- − 15°. Fig. 8a–d demonstrate the gripping process and Fig. 8e–h show the set-down process. With the electromagnet energized, the inhomogeneous magnetic field affected the closer part of the gripper more. The strips for different samples would bend to different directions due to the different orientations of the internal particle chains, which resulted in the open state of the gripper (Fig. 8a and b). Then, when the electromagnet was powered off, the strips would bend back to their initial state, which caused the target item, the blue stick, be gripped (Fig. 8c). After that, the item could be taken away to the destination (Fig. 8d). The video of whole grip process was supplied in support information (Movie S1).

Supplementary data related to this article can be found at https://doi.org/10.1016/j.compscitech.2020.108079.

## 5. Conclusion

In this paper, the off-axial anisotropic MR elastomers with different particle chain orientations were prepared. The mechanical properties under quasi-static and dynamic shear deformation were experimentally explored. The results showed that the larger the orientation angle of the particle chain is, the larger the magneto-induced shear modulus and the MR effect are. A modified magnetic dipole theoretical model was proposed to verify the experimental results. The mechanical properties are affected by the loading direction due to the orientation of off-axial particle chain inside the MR elastomers. When the A-MRE-0° sample is sheared in the N direction or in the P direction, the shear modulus is same. While for the A-MRE-θ ($\theta \neq 0$) sample, the shear modulus in the N direction is larger than that in the P direction. A mechanism was put forward to explain the results phenomenologically. The magneto-deformation of the off-axial anisotropic MR elastomers was also discussed. The experimental results revealed that the magneto-induced torque and normal force of this special MR elastomer could be significantly affected by the orientation of the aligned particle chains. Finally, several soft structures were designed and demonstrated by using the special anisotropic MR elastomer A-MRE-15°. It exhibited excellent application potential in the research of controllable shape morphing smart device.

## Acknowledgment

Financial supports from the National Natural Science Foundation of China (Grant No. 11572309,11972337, 11972343), the Strategic Priority Research Program of Chinses Academy of Sciences (Grant No. XDB22040502), and the Fundamental Research Funds for the Central Universities (WK2090000015) are gratefully acknowledged. This study was also supported by the Collaborative Innovation Center of Suzhou Nano Science and Technology.

## Appendix A. Supplementary data

Supplementary data to this article can be found online at https://doi.org/10.1016/j.compscitech.2020.108079.

## References


[1] S.R. Khimi, K.L. Pickering, Comparison of dynamic properties of magnetorheological elastomers with existing antivibration rubbers, Composites Part B 83 (2015) 175–183.

[2] A. Dominguez, R. Sedaghati, I. Stiharu, Modeling and application of MR dampers in semi-adaptive structures, Comput. Struct. 86 (3–5) (2008) 407–415.

[3] M. Ramalingam, R. Patel, M.A. Thirumurugan, D.D. Jebaseelan, C. Jebaraj, Control policies used for semi-active damper for automotive seating system: a review, Int. J. Dyn. Control 7 (3) (2018) 1135–1148.

[4] M.H. Abu Bakar, A.Q. Alwi, Design and fabrication of a magneto-rheological fluid based torque sensor for automotive application, Adv. Eng. Proc. Technol. 102 (2019) 101–113.

[5] M. Schumann, J. Morich, T. Kaufhold, V. Bohm, K. Zimmermann, S. Odenbach, A mechanical characterisation on multiple timescales of electroconductive magnetorheological elastomers, J. Magn. Magn Mater. 453 (2018) 198–205.

[6] L. Ge, X. Gong, Y. Wang, S. Xuan, The conductive three dimensional topological structure enhanced magnetorheological elastomer towards a strain sensor, Compos. Sci. Technol. 135 (2016) 92–99.

[7] L. Yuan, S. Sun, Z. Pan, D. Ding, O. Gienke, W. Li, Mode coupling chatter suppression for robotic machining using semi-active magnetorheological elastomers absorber, Mech. Syst. Signal Process. 117 (2019) 221–237.

[8] G. Liao, X. Gong, S. Xuan, Phase based stiffness tuning algorithm for a magnetorheological elastomer dynamic vibration absorber, Smart Mater. Struct. 23 (1) (2014), 015016.

[9] H. Deng, X. Gong, L. Wang, Development of an adaptive tuned vibration absorber with magnetorheological elastomer, Smart Mater. Struct. 15 (5) (2006) N111–N116.

[10] Y. Sun, Y. Wang, J. Yao, L. Gao, D. Li, Y. Liu, Highly magnetic sensitivity of polymer nanocomposite hydrogels based on magnetic nanoparticles, Compos. Sci. Technol. 141 (2017) 40–47.

[11] L. Chen, X. Gong, W. Li, Microstructures and viscoelastic properties of anisotropic magnetorheological elastomers, Smart Mater. Struct. 16 (6) (2007) 2645–2650.

[12] X. Guan, X. Dong, J. Ou, Magnetostrictive effect of magnetorheological elastomer, J. Magn. Magn Mater. 320 (3–4) (2008) 158–163.

[13] O.V. Stolbov, Y.L. Raikher, M. Balasoiu, Modelling of magnetodipolar striction in soft magnetic elastomers, Soft Matter 7 (18) (2011) 8484–8487.

[14] R. Elhajjar, C.-T. Law, A. Pegoretti, Magnetostrictive polymer composites: recent advances in materials, structures and properties, Prog. Mater. Sci. 97 (2018) 204–229.

[15] C. Rodríguez, M. Rodriguez, I. Orue, J.L. Vilas, J.M. Barandiarán, M.L.F. Gubieda, L.M. Leon, New elastomer–Terfenol-D magnetostrictive composites, Sens. Actuators, A 149 (2) (2009) 251–254.

[16] M.D. Christie, S.S. Sun, D.H. Ning, H. Du, S.W. Zhang, W.H. Li, A torsional MRE joint for a C-shaped robotic leg, Smart Mater. Struct. 26 (1) (2017), 015002.

[17] H. Xu, M. Medina-Sanchez, V. Magdanz, L. Schwarz, F. Hebenstreit, O.G. Schmidt, Sperm-hybrid micromotor for targeted drug delivery, ACS Nano 12 (2018) 327–337.

[18] J. Yao, Y. Sun, Y. Wang, Q. Fu, Z. Xiong, Y. Liu, Magnet-induced aligning magnetorheological elastomer based on ultra-soft matrix, Compos. Sci. Technol. 162 (2018) 170–179.

[19] X. Zhao, J. Kim, C.A. Cezar, N. Huebsch, K. Lee, K. Bouhadir, D.J. Mooney, Active scaffolds for on-demand drug and cell delivery, Proc. Natl. Acad. Sci. U.S.A. 108 (1) (2011) 67–72.

[20] R.V. Ramanujan, L.L. Lao, The mechanical behavior of smart magnet–hydrogel composites, Smart Mater. Struct. 15 (4) (2006) 952–956.

[21] F. Tsumori, A. Saijou, T. Osada, H. Miura, Development of actuation system for artificial cilia with magnetic elastomer, Jpn. J. Appl. Phys. 54 (2015), 06FP12.

[22] T.A. Duenas, G.P. Carman, Particle distribution study for low-volume fraction magnetostrictive composites, J. Appl. Phys. 90 (5) (2001) 2433–2439.

[23] S. Abramchuk, E. Kramarenko, G. Stepanov, L.V. Nikitin, G. Filipcsei, A. R. Khokhlov, M. Zrínyi, Novel highly elastic magnetic materials for dampers and seals: Part I. Preparation and characterization of the elastic materials, Polym. Adv. Technol. 18 (11) (2007) 883–890.

[24] S. Abramchuk, E. Kramarenko, D. Grishin, G. Stepanov, L.V. Nikitin, G. Filipcsei, A. R. Khokhlov, M. Zrínyi, Novel highly elastic magnetic materials for dampers and seals: part II. Material behavior in a magnetic field, Polym. Adv. Technol. 18 (7) (2007) 513–518.

[25] N.T. Lai, H. Ismail, M.K. Abdullah, R.K. Shuib, Optimization of pre-structuring parameters in fabrication of magnetorheological elastomer, Arch. Civ. Mech. Eng. 19 (2) (2019) 557–568.

[26] A.V. Bodnaruk, A. Brunhuber, V.M. Kalita, M.M. Kulyk, P. Kurzweil, A.A. Snarskii, A.F. Lozenko, S.M. Ryabchenko, M. Shamonin, Magnetic anisotropy in magnetoactive elastomers, enabled by matrix elasticity, Polymer 162 (2019) 63–72.

[27] M. Lallart, G. Sebald, G. Diguet, J.-Y. Cavaille, M. Nakano, Anisotropic magnetorheological elastomers for mechanical to electrical energy conversion, J. Appl. Phys. 122 (10) (2017) 103902.

[28] T. Tian, M. Nakano, Fabrication and characterisation of anisotropic magnetorheological elastomer with 45 degrees iron particle alignment at various silicone oil concentrations, J. Intell. Mater. Syst. Struct. 29 (2) (2018) 151–159.

[29] A. Boczkowska, S.F. Awietjan, S. Pietrzko, K.J. Kurzydłowski, Mechanical properties of magnetorheological elastomers under shear deformation, Composites Part B 43 (2) (2012) 636–640.

[30] L. Chen, X. Gong, W. Jiang, J. Yao, H. Deng, W. Li, Investigation on magnetorheological elastomers based on natural rubber, J. Mater. Sci. 42 (14) (2007) 5483–5489.

[31] W. Li, M. Nakano, Fabrication and characterization of PDMS based magnetorheological elastomers, Smart Mater. Struct. 22 (5) (2013), 055035.

[32] R. Rosensweig, Ferrohydrodynamics, Cambridge University Press, Cambridge, 1985.

[33] M.R. Jolly, J.D. Carlson, B.C. Muñoz, T.A. Bullions, The magnetoviscoelastic response of elastomer composites consisting of ferrous particles embedded in a polymer matrix, J. Intell. Mater. Syst. Struct. 7 (6) (1996) 613–622.

[34] M. Zhu, M. Yu, S. Qi, J. Fu, Investigations on response time of magnetorheological elastomer under compression mode, Smart Mater. Struct. 27 (5) (2018), 055017.

[35] S. Qi, H. Guo, J. Fu, Y. Xie, M. Zhu, M. Yu, 3D printed shape-programmable magneto-active soft matter for biomimetic applications, Compos. Sci. Technol. 188 (2020) 107973.